Applied Surface Science 681 (2025) 161600

Contents lists available at ScienceDirect

Applied Surface Science

journal homepage: www.elsevier.com/locate/apsusc

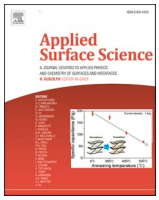

Full Length Article

High entropy 2D metals sulfides: Fast synthesis, exfoliation and electrochemical activity in overall water splitting at alkaline pH

Vladislav Buravets [a], Elena Miliutina [a], Vasilii Burtsev [a], Kamil Severa [a], Vera Shilenko [a], Jana Rosenkranzova [a], Philipp Hönicke [b,c], Tomáš Hrbek [d], Vaclav Svorcik [a], Oleksiy Lyutakov [a,*]

[a] Department of Solid State Engineering, University of Chemistry and Technology, 16628 Prague, Czech Republic
[b] Helmholtz-Zentrum Berlin, Hahn-Meitner Platz 1, 14109 Berlin, Germany
[c] Physikalisch-Technische Bundesanstalt (PTB), Abbestr. 2-12, 10587 Berlin, Germany
[d] Department of Surface and Plasma Science, Faculty of Mathematics and Physics, Charles University, 180 00 Prague, Czech Republic

ARTICLE INFO

Keywords:
High entropy sulfides
Overall water splitting
HER
OER

ABSTRACT

Novel simple and efficient method for synthesis of 2D high entropy sulfides of iron group metals is described. The method utilizes inorganic salts as precursors and CS_2 as a sulfurizing agent, which makes it possible to achieve high entropy composition through combination of freezing of the precursor solution, subsequent freeze-drying step, sulfurization, and exfoliation in liquid nitrogen. The created material was investigated as a catalyst for electrochemical water splitting at different pH. Measured overpotentials at 10 and 100 mA*cm^{-2} current densities for hydrogen evolution reaction (HER) were found to be 49 and 315 mV respectively, while for oxygen evolution reaction (OER) the overpotentials required for reaching 10 and 100 mA*cm^{-2} current densities were 370 and 591 mV respectively, both in 1 M KOH solution. The Tafel slopes for HER were found to be 235, 105, and 111 mV/dec in basic, neutral, and acidic conditions, respectively, while only 63 mV/dec for OER in basic conditions. The calculated values of the turnover frequency were *0.62 s^{-1}* for HER and *0.10 s^{-1}* for OER. We also confirmed the key role of high entropy in the catalytic activity of the material by excluding individual elements from the composition of the HES.

1. Introduction

High entropy materials started with ambitious alloy obtained by Brian Cantor at the beginning of the 21st century [1]. Since then, significant interest of such materials was stimulated by theoretical and experimental observations of their unique properties, including high (electro)catalytic activity [2–5]. Following research extends these ideas to other types of materials such as oxides, nitrides, carbides, borides, and sulfides [6–10]. Combined with other achievements of materials science (e.g. 2D structures), synergy of all these concepts can provide results with possible applications in broad fields [11]. In particular, high entropy materials demonstrate huge potential in the process of water splitting [12]. After the development of the descriptors for the electrochemical processes, significant progress in the catalyst design was achieved, with binding energies of the reactants/products being the most reliable factor to tune the catalytic activity [13–23]. Since the adsorption energy of an active site is a result of the site identity including short- and long-range interactions of the neighbouring atoms immense flexibility of the binding energy can be obtained from the material with highly entropic elemental distribution [2,4,5,24]. Therefore, the high entropy materials are considered as ideal catalysts for electrochemical water splitting. They can replace, or even outperform, both hydrogen and oxygen evolution reactions traditional rare metal-based catalysts without the loss of overall process efficiency and materials durability [25].

However, achieving high entropy is generally difficult because of the diverse physical properties of mixed materials caused by clusterization. Other complications arise with nonmetallic materials, the synthesis of which is another challenge itself due to scalability, time, and equipment requirements, as well as poor phase control [26–28]. In particular, few synthesis routes were suggested to achieve high entropy in such materials; however, entropy-driven reversibility by low temperature equilibration might be another complication to obtain such materials [29]. For high entropy sulfides, these limitations are further extended, since they require long-term (order of days) synthesis in a quartz ampoule or the usage of hazardous substances such as HF, including high

* Corresponding author.
E-mail address: lyutakoo@vscht.cz (O. Lyutakov).

https://doi.org/10.1016/j.apsusc.2024.161600
Received 4 July 2024; Received in revised form 15 October 2024; Accepted 20 October 2024
Available online 21 October 2024

temperatures (>1200 °C) [6,30,31]. Only recently, alternative synthesis routes have been proposed for the preparation of high entropy sulfides, which still require precursor synthesis to prevent metal cations to clusterize by utilising organic molecules [32].

In order to tackle this problem of synthesis routes for high entropy sulfides, we modify our method of sulfurization which can be based on a simple method by using CS_2 as a strong sulfurizing agent that requires only quartz flow-through reactor, furnace, and argon as a carrier gas [33,34]. In this work, we show a fast (only 2 h) and low-temperature sulfurization method, which uses metal salts as precursors. For entropy stabilization, an aqueous solution of the precursor salts is frozen in liquid nitrogen, freeze-dried, and sulfurized in the reactor. The applicability of this new route was demonstrated in the synthesis of Cr-Fe-Ni-Co-Zn-S. Furthermore, we show that a 2D structure can be achieved for the synthesized high entropy sulfide by exfoliation in liquid nitrogen. The 2D (CrFeNiCoZn)S system was shown to be a promising catalyst for the overall water splitting in alkaline media.

2. Experimental

Detailed description of the used materials, samples preparation and characterization is given in Supporting Information (SI). Briefly, equimolar amounts of Cr, Fe, Co, Ni, and Zn salts were dissolved in water and frozen using liquid nitrogen, resulting in the immediate solidification into ice, containing a highly entropic salt. The resulting "ice" was subsequently subjected to freeze-drying, yielding the dry high entropy salt containing the corresponding metal salts. In the subsequent step, the resulting powder was rapidly transferred into a hot zone of quartz reactor continuously filled with CS_2 [33,34]. The synthesis procedure produced a black powder that underwent further investigation. The created powder was then exfoliated and subjected to X-ray diffraction, atomic force microscopy (AFM), scanning electron and high-resolution transmission electron microscopies (SEM and HR-TEM, respectively) coupled with energy dispersive X-ray spectroscopy, and Raman analysis. In addition, reference-free grazing incidence X-ray fluorescence [35] based quantification was carried out at the four-crystal monochromator beamline [36] at the BESSY II electron storage ring. Here, physically calibrated instrumentation [37] is used to perform a quantitative analysis of recorded X-ray fluorescence spectra without the need for any reference material. For these experiments, the powders were drop casted on pieces of silicon wafers.

Electrochemical measurements were carried out using Palm Sens 4 potentiostat (Palm Instruments, Netherlands) controlled by the PSTrace 5.9 program using a three-electrode, two-compartment electrochemical cell (H-type). Measurements were performed in acidic (0.5 M H_2SO_4), alkaline (1 M KOH), and neutral (1 M PBS) electrolytes at HER and OER potentials.

3. Results and discussion

Main experimental concept of high entropy sulfides preparation is schematically presented in Fig. 1. In the first step the high-entropy mixture of Cr, Fe, Co, Ni and Zn salts was created using rapid freezing of corresponding solution and freeze-drying, which allows to conserve the entropic configuration of precursors. In the subsequent step, sulfurization was carried out. At this stage, it was important to prevent metals the clusterization and to subsequently ensure the high entropy structure of the product. Thus, sulfurization was performed by rapid heating of metals salt powder in CS_2 vapours, using blistering moving of initial powder from cold to hot reactor zone [33,34]. According to our initial assumption under these experimental conditions, the high entropy sulfide should be created and elemental clusterization prevented (see Fig. S1). In the next step, exfoliation in liquid nitrogen was performed to convert the created sulfide into a 2D structure with high surface and high catalytically active surface area [38,39]. The material was finally tested as HER and OER catalysts at various pH.

To evaluate and confirm the high-entropy nature and overall quality of the obtained material, a range of analytical methods was employed. The well-resolved peaks on the measured XRD pattern (Fig. 2A) suggests a high degree of material crystallinity. Owing to the presence of five metals, with relatively similar atomic sizes, the observed crystal structure shows a wide variety of materials characterized by the common formula AB_2S_4, where A and B represent metals with different oxidation states, 2 + or 3+, respectively and/or the possibility of A = B. The major phase (89 %) corresponds well to linnaeite group structure, which can be described by the formula AB_2S_4 with A, B = Co, Cu, Fe, Ni[40]. The presence of the minor phase (11 %) corresponds well to the structure of greigite, a cubic form of AB_2S_4, composed of one or a mixture of the iron group metal sulfides and suggested to be one of the crucial catalysts in the nature[41]. Similar structural arrangement aligns well with a variety of minerals found in nature with the aforementioned stoichiometry, including Mn, Cr, Fe, Zn, Co, Ni, Fe, Cu, Cd and exhibiting similar crystal

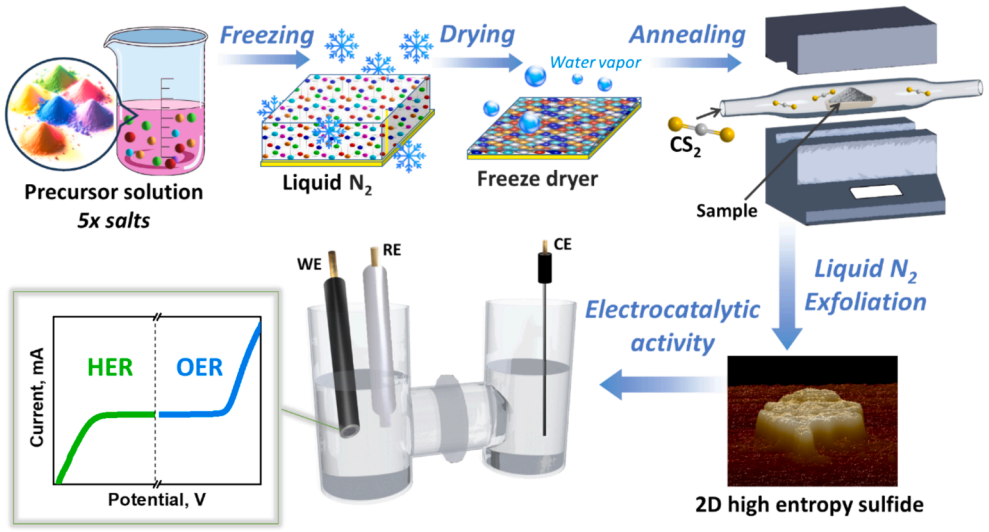

Fig. 1. Synthesis workflow for High Entropy Sulfides (HES) of iron group metals. In the first step, the mixture of the metal salts in aqueous solution underwent express freezing and solidification in liquid N_2 followed by freeze-drying. In the next step the rapid sulfurization of the obtained powder (salts mixture) was performed in a tube furnace by rapid transfer of the powder into the hot zone of the reactor purged with Ar/CS_2. Post-treatment consisted of exfoliation in liquid N_2 to achieve a 2D material structure. Finally, water splitting electrocatalytic activity of prepared sulfides at different pH were tested.

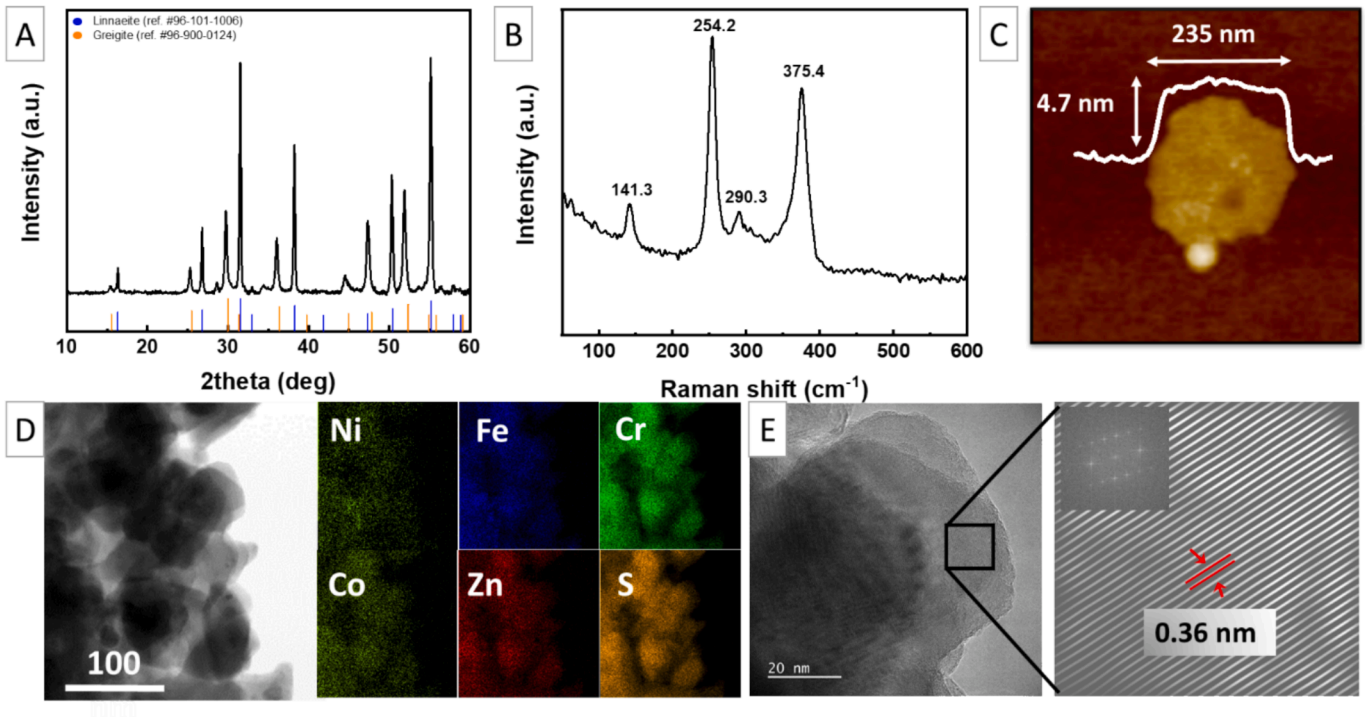

Fig. 2. Morphological and structural characterization of HES. (A) – XRD, (B) – Raman spectroscopy, (C) – AFM, (D) – TEM-EDX and (E) – HRTEM and corresponding FFT.

structures [42].

The Raman spectroscopy (Fig. 2B) unveils sharp peaks at 141, 254, 290, and 375 cm^{-1}, which correspond well with the formed sulfides [43]. The last three peaks can be attributed to E1, E2, and A1 vibrational modes, while the peak at 141 may be due to the intercalation of an additional metal (A) into the structure, resulting in AB_2S_4 where B stands for the same or another metal identity [44], which is in good agreement with the XRD results. Finally, the homogeneous entropic distribution of elements after the sulfurization and absence of clustering was subsequently confirmed by scanning electron microscopy combined with energy dispersive X-ray spectroscopy (SEM-EDX – see Fig. S2).

In the final preparation step, the materials were exfoliated into 2D structure using liquid nitrogen (Fig. 1). To assess the 2D structure of the exfoliated material, atomic force microscopy (AFM) analysis was conducted (Fig. 2C). In turn, several AFM images measured on independently prepared samples are presented in Fig. S3, definitively confirming the 2D structure of created material. The typical flake lateral dimension was around 200 nm and the thickness of about 4 nm, thereby confirming the 2D structure of the obtained sulfide.

TEM combined with EDX was employed to analyse the morphology of the obtained flakes and the corresponding distribution of the elements (Fig. 2D, E) as well as for confirming the correct HES structure. The images show that the obtained flakes are composed of Ni, Fe, Cr, Co, Zn, and S, which are well and homogeneously dispersed throughout the material. Importantly, no signs of clustering were observed, confirming that the material preserved a high-entropy elemental distribution. The lattice fringe spacing (Fig. 2E) was found to be 0.36 nm, which corresponds to the (220) plane and is in good agreement with the literature [6]. The slightly expanded structure in comparison with linnaeite (0.33 nm) and greigite (0.35 nm) can be explained by the presence of larger atoms, such as Ni and Zn, which was also reported for HES.

In the final step, the 2D high entropy sulfides (HESs) were analysed using X-ray photoelectron and X-ray fluorescence (XPS and XRF) spectroscopies. From the XRF spectrum (Fig. 3A) and a corresponding reference-free analysis, the composition of HESs was quantified as $Cr_{0.27}Fe_{0.29}Ni_{0.26}Co_{0.28}Zn_{0.04}S$. Therefore, the equimolar amounts of Cr, Fe, Ni, and Co were conserved while a part of Zn was lost, probably as a result of its sublimation due to the low melting point of $ZnCl_2$ (290 °C) and its evaporation in the reaction chamber. In turn, survey XPS spectrum also reveals the coexistence of Ni, Co, Fe, Cr, Zn and S in the composition of HESs (Fig. S4). More informative high-resolution XPS spectra of particular elements were recorded and presented in Fig. 3 B-G. Detailed analysis of XPS spectra given in SI, indicating that Ni, Fe, and Co co-exists in two oxidation states (2 + and 3 +), while for Zn a single oxidation state is observed. For Cr, two oxidation states are also present, presumably also 2 + and 3 + . In the case of sulfur, two peaks corresponding to S $2p_{3/2}$ and S $2p_{1/2}$ are recorded at the positions of 161.1 and 162.3 eV, respectively and assigned to metal-sulfur bonds (162.3 eV) and low coordinated sulfur at the surface (161.1 eV) [45,46].

Generally, the performed measurements confirmed the ability of the HES preparation in the form of 2D flakes. The proposed route is relatively simple and quick. To further highlight this issue, we compared our approach with those previously published [6,32,47–53]. The results of the comparison are summarized in Table 1. As is evident, the proposed approach is favored by a relatively short preparation time. Moreover, in comparison to most of published works, a lower temperature can be used. In addition, our method does not require unique equipment, since the main steps can be realized with the utilization of lyophilizer and blow-off furnace.

4. Electrochemical investigation

The catalytic activity of the obtained $Cr_{0.27}Fe_{0.29}Ni_{0.26}Co_{0.28}Zn_{0.04}S$ (HES) was further investigated in water splitting, both OER and HER. Since the electrocatalytic performance significantly depends on the acidity, measurements were conducted in three different media – acidic (0.5 M H_2SO_4, pH = 0.1), neutral (1 M phosphate buffer saline (PBS), pH = 7.4) and basic (1 M KOH, pH = 13), see Fig. 4 and Fig. S5.

Firstly, linear sweep voltammetry (LSV) curves indicate a moderate HER catalytic performance of the created material in all the media used (Fig. S5). With acidic electrolyte in particular, the onset potential of −0.25 V vs RHE and 373 mV overpotential required to achieve current

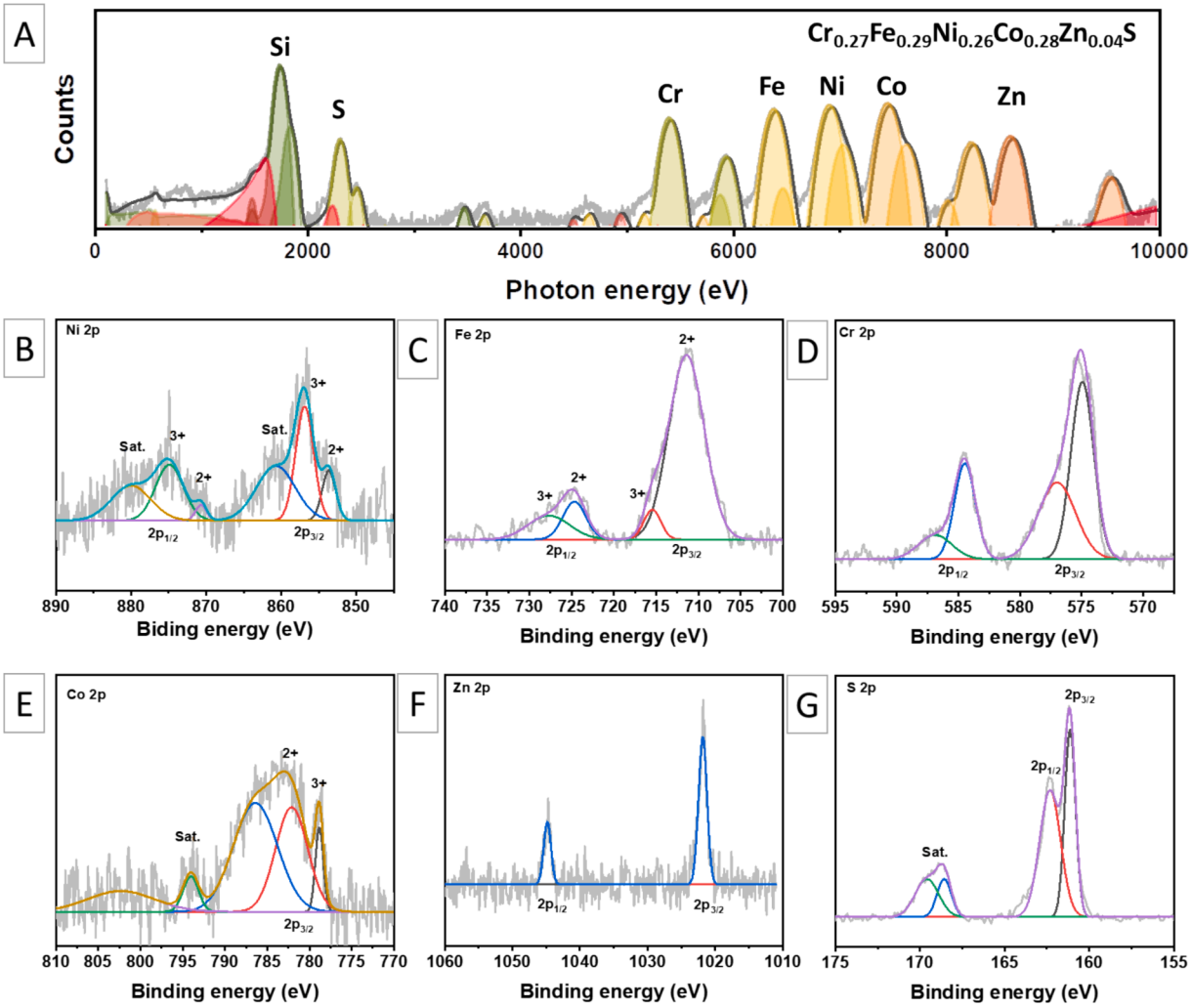

Fig. 3. (A) – High energy XRF analysis of elemental composition of HES. High resolution XPS for Ni (B), Fe (C), Cr (D), Co (E), Zn (F), and S (G).

Table 1
Comparison of various synthetic approaches used for HES preparation with the method proposed in this work.

High entropy sulfide + E4: J14	Synthetic route	Synthesis time	Precursor	Comments	Reference
$(CuSnMgGeZn)S_9$,	Ball milling + annealing	60 h	metal sulfides	60 h. ball milling and sintering at 750 °C and 50 MPa	[47]
$(FeNiCoCrCuAlMn)S_{xx}$,	Solvothermal	18 h	metal salts	Annealing of metal salts followed by introduction of sulphur source	[48]
$(Cr_xMn_yFe_zCo_qTi_mCr_nNi_q)S_x$	Pulsed thermal decomposition	6 h	metal salts	Decomposition of metal salts with thiourea at 1650 K.	[6]
	High energy ball milling of metal sulfides	110 h / 60 h	metal sulfides	Ball milling for various time in dependence of composition	[49]
(ZnCoCuInGa)S	Element exchange	2 h	metal sulfide	Multication exchange starting from the Cu1.8S	[50]
(CuAgZnCoMnInGa)S	Synthesys of metal diethyldithiocarbamate + annealing	13 h	metal salts	Synthesis of metal diethyldithiocarbamate and annealing in Ar at 500 °C	[32]
$(Ti_xFe_yCo_zNi_qMo_nMn_m)S_{5-12}$,	ball milling under Ar	14 h	metal sulfides	Ball milling of metal sulfide powders	[51]
$(FeCoNiCuRu)S_2$	High pressure and high temerature + ball milling	12 h	elemental metals and sulfur	Synthesis was performed at 1400 °C and high pressure (5 GPa cubic press), followed by ball milling for 10 h.	[52]
(FeCoNiMoAl)S	Thermal injection	< 2h	metal acetylacetonate and sulfur	Dissolving metal acetylacetonates in oleylamine and oleic acid and addition of dissolved sulfur at 330 °C	[53]
(CrFeNiCoZn)S	Thermal solid–gas sulfurization	2 h	inorganic metal salts	Sulfurization of metal salts by CS_2 in tube furnace at 500 °C	***this work***

density of 10 $mA*cm^{-2}$ were observed. Activity in basic pH and neutral conditions was even lower – overpotentials of 435 mV and 464 mV were required for 10 $mA*cm^{-2}$ in basic and neutral conditions (corresponding Tafel slopes were calculated to be 102, 115 and 148 $mV*dec^{-1}$ in acidic, neutral and basic conditions – Fig. S5B). Such catalytic performance cannot be considered as satisfactory, taking into account the latest results obtained in the field of rare metal-free HER catalysts [33,45,54,55]. However, during the stability tests the apparent decrease

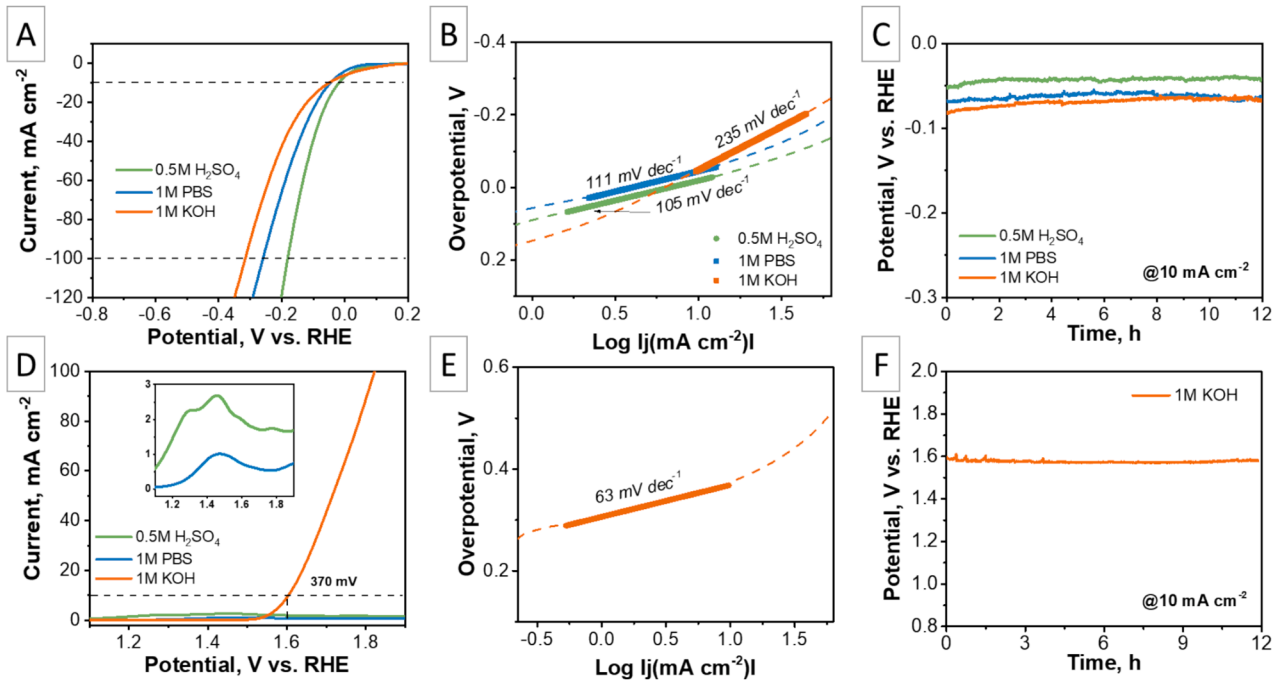

Fig. 4. Catalytic performance of HES in water splitting: HER (A-C) and OER (D-F) in different pH conditions. LSV curves – (A) and (D); Tafel slopes – (B) and (E); stability test, performed at 10 mA*cm^{-2} for 12 h – (C) and (F). The results are valid for as-prepared flakes in OER potentials and for activate flakes in HER potentials.

of potential required to maintain a constant current density was observed in acidic conditions. Such phenomenon can be associated with the material's electrochemical self-activation and improvement of its HER performance [33,56]. Thus, in the next step the HES flakes were subjected to electrochemical self-activation (performed in acidic condition in an H-type cell with Nafion membrane). Electrocatalytic performance of the activated HES was subsequently tested in neutral and alkaline conditions (taking into account the OER results, as described below).

HER performance of the activated HES are presented in Fig. 4 A-C. Overpotentials required for reaching 10 and 100 mA*cm^{-2} were 15 and 180 mV, 49 and 260 mV, 49 and 316 mV in acidic, neutral and alkaline electrolytes, respectively. Calculated Tafel slopes were 105, 111 and 235 mV*dec^{-1}. Such catalytic performance can be considered satisfactory and comparable with recent results reached in the field of rare metal-free HER catalysts [33,45,54,55]. This is especially true for alkaline conditions where technology is much better established from the industrial perspective [57–59]. The evaluated stability curve, measured in alkaline conditions as presented in Fig. 4C, indicates catalytic activity remains at the same level, i.e. without its subsequent increase or worsening. Finally, it should also be noted that previous flakes' activation resulted in a complete loss of catalytic OER activity (Fig. S6 and results below).

To evaluate the OER performance, similar electrochemical tests were performed with utilization of as-prepared HES flakes (Fig. 4, D-F). First, in acidic and neutral conditions, small oxidative peak was observed at approximately 1.5 V vs. RHE, suggesting oxidation of the material is taking place. Similar findings were already reported for the sulfides of the iron group metals [60,61]. Further increases in the overpotential in acidic and basic media do not result in the current increase up to potential of 1.9 V vs RHE, suggesting a surface blockage due to oxidation occurred, hindering the OER.

However, LSV analysis reveals that HES performance requires 370 mV to reach the current density of 10 mA*cm^{-2} and 591 mV to reach 100 mA*cm^{-2} in 1 M KOH electrolyte. Besides, Tafel slope (Fig. 4E) of HES in basic electrolyte is only 63 mV*dec^{-1}, which is a superior value to most of the previously reported non-precious metal OER [61]. Furthermore, HES exhibits excellent durability in basic conditions since the potential was stable and slightly below 1.6 V vs. RHE to deliver 10 mA*cm^{-2} (Fig. 4F).

Taking into account the present HER (reached with activated 2D HES flakes) and OER results (reached with as prepared 2D HES flakes) and comparing HES performance with those reported in literature [6,62–65] we can conclude than our material exhibits remarkable activity in the basic conditions and can be considered a promising catalyst for the overall water splitting reaction. The observed catalytic activity can be explained by the so-called cocktail effect, commonly observed in high entropy materials. In other words, the enhancement of redox activity can be attributed to the wide variety of electronic constructions on the HES surface, which according to the d-band adsorption theory allows a near-continuous distribution of adsorbed energy and creation of various highly active sites[6,12,66]. It should also be noted that the redox properties of a HES are a strong function of synergistic interactions between neighboring atoms, mixed in a random way [67]. As a result, the great variability of active sites stabilize HER or OER intermediates that are commonly unstable on a „single" metal surface.

Moreover, the calculated values of mass activity (see Supporting Information) were estimated to be 5.4 A/mg for OER, performed in alkaline conditions, which value can be considered as a good results. In turn, for HER the mass activity varied with pH changes. In particular, 10.3, 5.8, and 6.2 A/mg were reached for acidic, alkaline, and neutral pH, respectively. We also calculated the turnover frequency as an important electrochemical parameter, revealing the material catalytic activity. In this case, it should be noted that the direct estimation of the number of active surface sites, where HER or OER can proceed is complicated by the fact that we deal with high entropy materials [67] in which the reaction can proceed on various active sites determined by a close proximicity of different atoms. Thus, in this case we used the experimental routes proposed in [68,69], based on the measurements of the number of active sites and the subsequent TOF calculation. The results obtained were TOF(S^{-1}) = $0.62\ s^{-1}$ (@0.05 V vs. RHE) for HER and TOF(S^{-1}) = $0.1\ s^{-1}$ (@1.6 V vs. RHE) for OER. Such values can also be considered as good ones, compared to data from the literature[6,51].

Regarding the particular HES composition, we can suggest that the

good redox activity of high-entropy iron group metal sulfides in alkaline pH environments may be due to their elemental composition (Fe, Ni, Co and their combinations provide the greatest catalytic activity, while Cr and Zn improve stability) [48,70,71] and electronic structure, which possesses enhanced configurational entropy [6,50] and various synergistic bonds between metallic elements favouring surface (oxy)hydroxide formation [48], improved conductivity and corrosion resistance [51]. Together, all these factors make them highly efficient and stable catalysts in alkaline environments for reactions such as OER and HER.

To check the impact of particular elements on the HES catalytic activity, a range of materials with one element missing was prepared (in particular – sulfides of ternary metal compounds Cr-Fe-Ni-Co, Cr-Fe-Ni-Zn, Cr-Fe-Co-Zn, Cr-Ni-Co-Zn, and Fe-Ni-Co-Zn). Their composition and structure were checked usingSEM-EDX and XRD measurements, both performed before flakes exfoliation (Fig. SX1 and Fig. SX2). Subsequently, the created sulfides were exfoliated and used for HER and OER measurements, both performed in alkaline conditions (Fig. SX3). For better clarity in the results interpretation, we also plotted the overpotentials at 10 mA/cm^2 for the both water-splitting half-reactions (Fig. SX4). The results indicate that a more noticeable decrease in HER activity was observed for missing Zn or Co elements. Removal of Fe and Ni elements led to a moderate decrease in HER activity, while the absence of Cr resulted in even less pronounced suppression of HER activity. It should be noted that in case of exclusion of any of the elements, we did not reach such great activity as in the HES case, which highlights the key role of all elements (in other words, so-called cocktail effects).

Similar experiments were performed with the utilization of Cr-Fe-Ni-Co, Cr-Fe-Ni-Zn, Cr-Fe-Co-Zn, Cr-Ni-Co-Zn, and Fe-Ni-Co-Zn sulfides in OER conditions (Fig. SX3 and Fig. SX4). In this case, the highest decrease in redox activity was observed in the absence of Ni in the material composition. In all other cases, the redox activity of the four-component materials was lower compared to HES, indicating that the cocktail effect plays a key role in the reaction proceeding on the surface of high–entropy material.

5. Conclusions

In this study, a novel method for synthesizing high entropy sulfides (HES) of iron group metals, exemplified by Cr, Fe, Ni, Co and Zn, is proposed. The benefit of the method lies in utilizing abundant inorganic salts as precursors and CS2 as a sulfurizing agent. To achieve a highly entropic composition, our method involves freezing of the precursor solution containing salts of corresponding metals, followed by a subsequent freeze-drying step. Sulfurization is efficiently carried out in a flow reactor by the rapid insertion of metals powder in the hot reactor zone. In the final stage, exfoliation in liquid nitrogen is employed to obtain a 2D morphology in the resulted HES. The structure and morphology of HES flakes was subsequently examined and confirmed using TEM, HRTEM, AFM, XPS, XRF, SEM-EDX and Raman techniques. Created material was tested as an electrocatalyst for water splitting at different pH. As prepared HES showed moderate catalytic activity towards HER. However, electrochemical self-activation, performed in acidic conditions results in a significant increase of 2D HES catalytic activity in water reduction, especially in alkaline conditions. The as-prepared HES flakes show good catalytic activity towards OER under alkaline conditions, even without pre-activation. Therefore, the created material can be considered as a good catalyst for overall (bifunctional) water splitting under alkaline conditions. To summarise, a ground-breaking route is presented for the synthesis of high entropy sulfides of non-precious metals with good catalytic properties, which could find practical applications in energy conversion and storage.

CRediT authorship contribution statement

Vladislav Buravets: Writing – review & editing, Methodology, Investigation, Data curation, Conceptualization. **Elena Miliutina:** Visualization, Validation, Methodology, Investigation. **Vasilii Burtsev:** Investigation. **Kamil Severa:** Investigation. **Vera Shilenko:** Investigation. **Jana Rosenkranzova:** Investigation. **Philipp Hönicke:** Methodology, Investigation. **Tomáš Hrbek:** Investigation. **Vaclav Svorcik:** Writing – review & editing, Validation, Formal analysis. **Oleksiy Lyutakov:** Writing – original draft, Validation, Supervision, Data curation.

Declaration of competing interest

The authors declare that they have no known competing financial interests or personal relationships that could have appeared to influence the work reported in this paper.

Acknowledgement

This work was supported by the Czech Science Foundation GACR under project no. 22-02022S and by the Project OP JAK_Eco&Stor, No CZ.02.01.01/00/22_008/0004617, of the Ministry of Education, Youth and Sports, which is co-funded by the European Union, in particular, Brussels requirement. The authors also acknowledge CERIC-ERIC Consortium for access to experimental facilities at LRI SPL-HTC in Prague (Proposal number: 20237251).

Appendix A. Supplementary data

Supplementary data to this article can be found online at https://doi.org/10.1016/j.apsusc.2024.161600.

Data availability

The data is available at https://doi.org/10.5281/zenodo.12608522

References

[1] B. Cantor, I.T.H. Chang, P. Knight, A.J.B. Vincent, Microstructural development in equiatomic multicomponent alloys, Mater. Sci. Eng. A 375–377 (2004) 213–218, https://doi.org/10.1016/j.msea.2003.10.257.
[2] T. Löffler, A. Ludwig, J. Rossmeisl, W. Schuhmann, What makes high-entropy alloys exceptional electrocatalysts? Angew. Chem. Int. Ed. 60 (2021) 26894–26903, https://doi.org/10.1002/anie.202109212.
[3] T.A.A. Batchelor, J.K. Pedersen, S.H. Winther, I.E. Castelli, K.W. Jacobsen, J. Rossmeisl, High-entropy alloys as a discovery platform for electrocatalysis, Joule 3 (2019) 834–845, https://doi.org/10.1016/j.joule.2018.12.015.
[4] V.A. Mints, J.K. Pedersen, A. Bagger, J. Quinson, A.S. Anker, K.M.Ø. Jensen, J. Rossmeisl, M. Arenz, Exploring the composition space of high-entropy alloy nanoparticles for the electrocatalytic H $_2$ /CO oxidation with bayesian optimization, ACS Catal. 12 (2022) 11263–11271, https://doi.org/10.1021/acscatal.2c02563.
[5] J.K. Pedersen, T.A.A. Batchelor, D. Yan, L.E.J. Skjegstad, J. Rossmeisl, Surface electrocatalysis on high-entropy alloys, Curr. Opin. Electrochem. 26 (2021) 100651, https://doi.org/10.1016/j.coelec.2020.100651.
[6] M. Cui, C. Yang, B. Li, Q. Dong, M. Wu, S. Hwang, H. Xie, X. Wang, G. Wang, L. Hu, High-entropy metal sulfide nanoparticles promise high-performance oxygen evolution reaction, Adv. Energy Mater. 11 (2021) 2002887, https://doi.org/10.1002/aenm.202002887.
[7] Y. Pan, J.-X. Liu, T.-Z. Tu, W. Wang, G.-J. Zhang, High-entropy oxides for catalysis: A diamond in the rough, Chem. Eng. J. 451 (2023) 138659, https://doi.org/10.1016/j.cej.2022.138659.
[8] J.-J. Wang, F.-Y. Ouyang, Oxidation behavior of Al-Cr-Nb-Si-Zr high entropy nitride thin films at 850 °C, Corros. Sci. 187 (2021) 109467, https://doi.org/10.1016/j.corsci.2021.109467.
[9] M.D. Hossain, T. Borman, C. Oses, M. Esters, C. Toher, L. Feng, A. Kumar, W. G. Fahrenholtz, S. Curtarolo, D. Brenner, J.M. LeBeau, J.-P. Maria, Entropy landscaping of high-entropy carbides, Adv. Mater. 33 (2021) 2102904, https://doi.org/10.1002/adma.202102904.
[10] X. Wang, Y. Zuo, S. Horta, R. He, L. Yang, A. Ostovari Moghaddam, M. Ibáñez, X. Qi, A. Cabot, CoFeNiMnZnB as a high-entropy metal boride to boost the oxygen evolution reaction, ACS Appl Mater. Interfaces 14 (2022) 48212–48219, https://doi.org/10.1021/acsami.2c11627.
[11] P.C.K. Vesborg, T.F. Jaramillo, Addressing the terawatt challenge: scalability in the supply of chemical elements for renewable energy, RSC Adv. 2 (2012) 7933, https://doi.org/10.1039/c2ra20839c.
[12] Y. Zhai, X. Ren, B. Wang, S.F. Liu, High-entropy catalyst—a novel platform for electrochemical water splitting, Adv. Funct. Mater. 32 (2022) 2207536, https://doi.org/10.1002/adfm.202207536.

[13] J.K. Nørskov, T. Bligaard, J. Rossmeisl, C.H. Christensen, Towards the computational design of solid catalysts, Nature Chem 1 (2009) 37–46, https://doi.org/10.1038/nchem.121.

[14] A. Vojvodic, J.K. Nørskov, New design paradigm for heterogeneous catalysts, Natl. Sci. Rev. 2 (2015) 140–143, https://doi.org/10.1093/nsr/nwv023.

[15] J.H. Montoya, L.C. Seitz, P. Chakthranont, A. Vojvodic, T.F. Jaramillo, J. K. Nørskov, Materials for solar fuels and chemicals, Nature Mater 16 (2017) 70–81, https://doi.org/10.1038/nmat4778.

[16] Y. Oh, J. Theerthagiri, M.L. Aruna Kumari, A. Min, C.J. Moon, M.Y. Choi, Electrokinetic-mechanism of water and furfural oxidation on pulsed laser-interlaced Cu2O and CoO on nickel foam, Journal of Energy Chemistry 91 (2024) 145–154, https://doi.org/10.1016/j.jechem.2023.12.023.

[17] H. Lee, J. Theerthagiri, M.L. Aruna Kumari, A. Min, C.J. Moon, V. Anbazhagan, R. L. Brutchey, M.Y. Choi, Leveraging phosphate group in Pd/PdO decorated nickel phosphate microflowers via pulsed laser for robust hydrogen production in hydrazine-assisted electrolyzer, Int. J. Hydrogen Energy 57 (2024) 176–186, https://doi.org/10.1016/j.ijhydene.2024.01.029.

[18] Y. Jeong, S.S. Naik, J. Theerthagiri, C.J. Moon, A. Min, M.L. Aruna Kumari, M. Y. Choi, Manifolding surface sites of compositional CoPd alloys via pulsed laser for hydrazine oxidation-assisted energy-saving electrolyzer: Activity origin and mechanism discovery, Chem. Eng. J. 470 (2023) 144034, https://doi.org/10.1016/j.cej.2023.144034.

[19] Y. Wu, Y. Wang, G. Sui, D. Guo, D. Chu, G. Xu, J. Li, Y. Li, D.-F. Chai, Cobalt nanoparticles intercalation coupled with tellurium-doping MXene for efficient electrocatalytic water splitting, J. Colloid Interface Sci. 675 (2024) 379–390, https://doi.org/10.1016/j.jcis.2024.07.025.

[20] S. Liang, G. Sui, D. Guo, Z. Luo, R. Xu, H. Yao, J. Li, C. Wang, g-C3N4-wrapped nickel doped zinc oxide/carbon core-double shell microspheres for high-performance photocatalytic hydrogen production, J. Colloid Interface Sci. 635 (2023) 83–93, https://doi.org/10.1016/j.jcis.2022.12.120.

[21] Y. Zhou, J. Gao, M. Ju, Y. Chen, H. Yuan, S. Li, J. Li, D. Guo, M. Hong, S. Yang, Combustion growth of NiFe layered double hydroxide for efficient and durable oxygen evolution reaction, ACS Appl. Mater. Interfaces 16 (2024) 28526–28536, https://doi.org/10.1021/acsami.4c03766.

[22] S. Liang, G. He, G. Sui, J. Li, D. Guo, Z. Luo, R. Xu, H. Yao, C. Wang, Z. Xing, ZIF-L-derived C-doped ZnO via a two-step calcination for enhanced photocatalytic hydrogen evolution, J. Mol. Struct. 1276 (2023) 134787, https://doi.org/10.1016/j.molstruc.2022.134787.

[23] S. Liang, G. Sui, J. Li, D. Guo, Z. Luo, R. Xu, H. Yao, C. Wang, S. Chen, ZIF-L-derived porous C-doped ZnO/CdS graded nanorods with Z-scheme heterojunctions for enhanced photocatalytic hydrogen evolution, Int. J. Hydrogen Energy 47 (2022) 11190–11202, https://doi.org/10.1016/j.ijhydene.2022.01.154.

[24] K. Li, W. Chen, Recent progress in high-entropy alloys for catalysts: synthesis, applications, and prospects, Mater. Today Energy 20 (2021) 100638, https://doi.org/10.1016/j.mtener.2021.100638.

[25] A. Amiri, R. Shahbazian-Yassar, Recent progress of high-entropy materials for energy storage and conversion, J. Mater. Chem. A 9 (2021) 782–823, https://doi.org/10.1039/D0TA09578H.

[26] Z. Sofer, D. Sedmidubský, J. Luxa, D. Bouša, Š. Huber, P. Lazar, M. Veselý, M. Pumera, Universal method for large-scale synthesis of layered transition metal dichalcogenides, Chem. Eur. J. 23 (2017) 10177–10186, https://doi.org/10.1002/chem.201701628.

[27] J. Theerthagiri, K. Karuppasamy, S.J. Lee, R. Shwetharani, H.-S. Kim, S.K.K. Pasha, M. Ashokkumar, M.Y. Choi, Fundamentals and comprehensive insights on pulsed laser synthesis of advanced materials for diverse photo- and electrocatalytic applications, Light Sci Appl 11 (2022) 250, https://doi.org/10.1038/s41377-022-00904-7.

[28] J. Theerthagiri, K. Karuppasamy, A. Min, D. Govindarajan, M.L.A. Kumari, G. Muthusamy, S. Kheawhom, H.-S. Kim, M.Y. Choi, Unraveling the fundamentals of pulsed laser-assisted synthesis of nanomaterials in liquids: Applications in energy and the environment, Appl. Phys. Rev. 9 (2022) 041314, https://doi.org/10.1063/5.0104740.

[29] C.M. Rost, E. Sachet, T. Borman, A. Moballegh, E.C. Dickey, D. Hou, J.L. Jones, S. Curtarolo, J.-P. Maria, Entropy-stabilized oxides, Nat Commun 6 (2015) 8485, https://doi.org/10.1038/ncomms9485.

[30] M.A. Buckingham, B. Ward-O'Brien, W. Xiao, Y. Li, J. Qu, D.J. Lewis, High entropy metal chalcogenides: synthesis, properties, applications and future directions, Chem. Commun. 58 (2022) 8025–8037, https://doi.org/10.1039/D2CC01796B.

[31] J. Cavin, A. Ahmadiparidari, L. Majidi, A.S. Thind, S.N. Misal, A. Prajapati, Z. Hemmat, S. Rastegar, A. Beukelman, M.R. Singh, K.A. Unocic, A. Salehi-Khojin, R. Mishra, 2D high-entropy transition metal dichalcogenides for carbon dioxide electrocatalysis, Adv. Mater. 33 (2021) 2100347, https://doi.org/10.1002/adma.202100347.

[32] W. Xiao, Y. Li, A. Elgendy, E.C. Duran, M.A. Buckingham, B.F. Spencer, B. Han, F. Alam, X. Zhong, S.H. Cartmell, R.J. Cernik, A.S. Eggeman, R.A.W. Dryfe, D. J. Lewis, Synthesis of high entropy and entropy-stabilized metal sulfides and their evaluation as hydrogen evolution electrocatalysts, Chem. Mater. 35 (2023) 7904–7914, https://doi.org/10.1021/acs.chemmater.3c00363.

[33] V. Buravets, F. Hosek, L. Lapcak, E. Miliutina, P. Sajdl, R. Elashnikov, V. Švorčík, O. Lyutakov, Beyond the platinum era—scalable preparation and electrochemical activation of TaS_2 flakes, ACS Appl. Mater. Interfaces 15 (2023) 5679–5686, https://doi.org/10.1021/acsami.2c20261.

[34] V. Buravets, F. Hosek, V. Burtsev, E. Miliutina, J. Maixner, L. Lapcak, L. Bajtosova, M. Cieslar, M. Procházka, J. Minar, Z. Kolska, V. Svorcik, O. Lyutakov, Rapid and universal synthesis of 2D transition metal (Ti, Zr, Hf, V, Nb, Ta, Cr, Mo, and W) sulfides through oxide sulfurization in CS2 vapor, Inorg. Chem. 63 (2024) 8215–8221, https://doi.org/10.1021/acs.inorgchem.4c00475.

[35] P. Hönicke, B. Detlefs, Y. Kayser, U. Mühle, B. Pollakowski, B. Beckhoff, Reference-free GIXRF-XRR as a methodology for independent validation of XRR on ultrathin layer stacks and a depth-dependent characterization, J. Vac. Sci. Technol. A 37 (2019) 041502, https://doi.org/10.1116/1.5094891.

[36] M. Krumrey, Design of a four-crystal monochromator beamline for radiometry at BESSY II, J Synchrotron Rad 5 (1998) 6–9, https://doi.org/10.1107/S0909049597011825.

[37] B. Beckhoff, Reference-free X-ray spectrometry based on metrology using synchrotron radiation, J. Anal. At. Spectrom 23 (2008) 845–853, https://doi.org/10.1039/B718355K.

[38] Y. Wang, Y. Liu, J. Zhang, J. Wu, H. Xu, X. Wen, X. Zhang, C.S. Tiwary, W. Yang, R. Vajtai, Y. Zhang, N. Chopra, I.N. Odeh, Y. Wu, P.M. Ajayan, Cryo-mediated exfoliation and fracturing of layered materials into 2D quantum dots, Sci. Adv. 3 (2017) e1701500.

[39] J. Zhang, Y. Wang, J. Cui, J. Wu, Y. Li, T. Zhu, H. Kang, J. Yang, J. Sun, Y. Qin, Y. Zhang, P.M. Ajayan, Y. Wu, Water-soluble defect-rich MoS_2 ultrathin nanosheets for enhanced hydrogen evolution, J. Phys. Chem. Lett. 10 (2019) 3282–3289, https://doi.org/10.1021/acs.jpclett.9b01121.

[40] J.F. Riley, Ferroan carrollites, cobaltian violarites, and other members of the linnaeite group: (Co, Ni, Fe, Cu)3S4, Mineral. Mag. 43 (1980) 733–739, https://doi.org/10.1180/minmag.1980.043.330.06.

[41] M.J. Russell, W. Martin, The rocky roots of the acetyl-CoA pathway, Trends Biochem. Sci 29 (2004) 358–363, https://doi.org/10.1016/j.tibs.2004.05.007.

[42] P. Škácha, J. Sejkora, J. Plášil, Z. Dolníček, J. Ulmanová, Grimmite, $NiCo_2S_4$, a new thiospinel from příbram, czech republic, Eur. J. Mineral. 33 (2021) 175–187, https://doi.org/10.5194/ejm-33-175-2021.

[43] S. Zhou, R. Wang, J. Han, D. Wang, H. Li, L. Gan, T. Zhai, Ultrathin non-van der waals magnetic rhombohedral Cr2S3: space-confined chemical vapor deposition synthesis and raman scattering investigation, Adv. Funct. Mater. 29 (2019) 1805880, https://doi.org/10.1002/adfm.201805880.

[44] S. Fan, S. Neal, C. Won, J. Kim, D. Sapkota, F. Huang, J. Yang, D.G. Mandrus, S.-W. Cheong, J.T. Haraldsen, J.L. Musfeldt, Excitations of intercalated metal monolayers in transition metal dichalcogenides, Nano Lett. 21 (2021) 99–106, https://doi.org/10.1021/acs.nanolett.0c03292.

[45] H. Liu, X. Ma, Y. Rao, Y. Liu, J. Liu, L. Wang, M. Wu, Heteromorphic NiCo2S4/Ni3S2/Ni foam as a self-standing electrode for hydrogen evolution reaction in alkaline solution, ACS Appl. Mater. Interfaces 10 (2018) 10890–10897, https://doi.org/10.1021/acsami.8b00296.

[46] X. Xiong, G. Waller, D. Ding, D. Chen, B. Rainwater, B. Zhao, Z. Wang, M. Liu, Controlled synthesis of NiCo2S4 nanostructured arrays on carbon fiber paper for high-performance pseudocapacitors, Nano Energy 16 (2015) 71–80, https://doi.org/10.1016/j.nanoen.2015.06.018.

[47] R.-Z. Zhang, F. Gucci, H. Zhu, K. Chen, M.J. Reece, Data-driven design of ecofriendly thermoelectric high-entropy sulfides, Inorg. Chem. 57 (2018) 13027–13033, https://doi.org/10.1021/acs.inorgchem.8b02379.

[48] T.X. Nguyen, Y.-H. Su, C.-C. Lin, J.-M. Ting, Self-reconstruction of sulfate-containing high entropy sulfide for exceptionally high-performance oxygen evolution reaction electrocatalyst, Adv. Funct. Mater. 31 (2021) 2106229, https://doi.org/10.1002/adfm.202106229.

[49] L. Lin, K. Wang, A. Sarkar, C. Njel, G. Karkera, Q. Wang, R. Azmi, M. Fichtner, H. Hahn, S. Schweidler, B. Breitung, High-entropy sulfides as electrode materials for li-ion batteries, Adv. Energy Mater. 12 (2022) 2103090, https://doi.org/10.1002/aenm.202103090.

[50] C.R. McCormick, R.E. Schaak, Simultaneous multication exchange pathway to high-entropy metal sulfide nanoparticles, J. Am. Chem. Soc. 143 (2021) 1017–1023, https://doi.org/10.1021/jacs.0c11384.

[51] L. Lin, Z. Ding, G. Karkera, T. Diemant, M.V. Kante, D. Agrawal, H. Hahn, J. Aghassi-Hagmann, M. Fichtner, B. Breitung, S. Schweidler, High-entropy sulfides as highly effective catalysts for the oxygen evolution reaction, Small Structures 4 (2023) 2300012, https://doi.org/10.1002/sstr.202300012.

[52] W. Cheng, J. Liu, J. Hu, W. Peng, G. Niu, J. Li, Y. Cheng, X. Feng, L. Fang, M.-S. Wang, S.A.T. Redfern, M. Tang, G. Wang, H. Gou, Pressure-stabilized high-entropy (FeCoNiCuRu)S2 sulfide anode toward simultaneously fast and durable lithium/sodium ion storage, Small 19 (2023) 2301915, https://doi.org/10.1002/smll.202301915.

[53] J. Shi, H. Jiang, X. Hong, J. Tang, Non-noble metal high entropy sulfides for efficient oxygen evolution reaction catalysis, Appl. Surf. Sci. 642 (2024) 158598, https://doi.org/10.1016/j.apsusc.2023.158598.

[54] A. Zabelina, E. Miliutina, D. Zabelin, V. Burtsev, V. Buravets, R. Elashnikov, V. Neubertova, M. Šťastný, D. Popelková, J. Lancok, S. Chertopalov, M. Paidar, A. Trelin, A. Michalcová, V. Švorčík, O. Lyutakov, Plasmon coupling inside 2D-like TiB2 flakes for water splitting half reactions enhancement in acidic and alkaline conditions, Chem. Eng. J. 454 (2023) 140441, https://doi.org/10.1016/j.cej.2022.140441.

[55] L. Lin, P. Sherrell, Y. Liu, W. Lei, S. Zhang, H. Zhang, G.G. Wallace, J. Chen, Engineered 2D transition metal dichalcogenides—a vision of viable hydrogen evolution reaction catalysis, Adv. Energy Mater. 10 (2020) 1903870, https://doi.org/10.1002/aenm.201903870.

[56] Y. Liu, J. Wu, K.P. Hackenberg, J. Zhang, Y.M. Wang, Y. Yang, K. Keyshar, J. Gu, T. Ogitsu, R. Vajtai, J. Lou, P.M. Ajayan, B.C. Wood, B.I. Yakobson, Self-optimizing, highly surface-active layered metal dichalcogenide catalysts for hydrogen evolution, Nat Energy 2 (2017) 17127, https://doi.org/10.1038/nenergy.2017.127.

[57] A.J. Shih, M.C.O. Monteiro, F. Dattila, D. Pavesi, M. Philips, A.H.M. da Silva, R. E. Vos, K. Ojha, S. Park, O. van der Heijden, G. Marcandalli, A. Goyal, M. Villalba, X. Chen, G.T.K.K. Gunasooriya, I. McCrum, R. Mom, N. López, M.T.M. Koper, Water electrolysis, Nat Rev Methods Primers 2 (2022) 1–19, https://doi.org/10.1038/s43586-022-00164-0.

[58] M. Ďurovič, J. Hnát, K. Bouzek, Electrocatalysts for the hydrogen evolution reaction in alkaline and neutral media, A Comparative Review, Journal of Power Sources 493 (2021) 229708, https://doi.org/10.1016/j.jpowsour.2021.229708.

[59] N. Mahmood, Y. Yao, J.-W. Zhang, L. Pan, X. Zhang, J.-J. Zou, Electrocatalysts for hydrogen evolution in alkaline electrolytes: mechanisms, Challenges, and Prospective Solutions, Advanced Science 5 (2018) 1700464, https://doi.org/10.1002/advs.201700464.

[60] Y. Hu, Y. Zheng, J. Jin, Y. Wang, Y. Peng, J. Yin, W. Shen, Y. Hou, L. Zhu, L. An, M. Lu, P. Xi, C.-H. Yan, Understanding the sulphur-oxygen exchange process of metal sulphides prior to oxygen evolution reaction, Nat Commun 14 (2023) 1949, https://doi.org/10.1038/s41467-023-37751-y.

[61] Y. Xue, Z. Zuo, Y. Li, H. Liu, Y. Li, Graphdiyne-supported NiCo2S4 nanowires: a highly active and stable 3D bifunctional electrode material, Small 13 (2017) 1700936, https://doi.org/10.1002/smll.201700936.

[62] Y. Kang, O. Cretu, J. Kikkawa, K. Kimoto, H. Nara, A.S. Nugraha, H. Kawamoto, M. Eguchi, T. Liao, Z. Sun, T. Asahi, Y. Yamauchi, Mesoporous multimetallic nanospheres with exposed highly entropic alloy sites, Nat Commun 14 (2023) 4182, https://doi.org/10.1038/s41467-023-39157-2.

[63] S.-Q. Chang, C.-C. Cheng, P.-Y. Cheng, C.-L. Huang, S.-Y. Lu, Pulse electrodeposited FeCoNiMnW high entropy alloys as efficient and stable bifunctional electrocatalysts for acidic water splitting, Chem. Eng. J. 446 (2022) 137452, https://doi.org/10.1016/j.cej.2022.137452.

[64] M. Plevová, J. Hnát, K. Bouzek, Electrocatalysts for the oxygen evolution reaction in alkaline and neutral media, A Comparative Review, Journal of Power Sources 507 (2021) 230072, https://doi.org/10.1016/j.jpowsour.2021.230072.

[65] C.C.L. McCrory, S. Jung, I.M. Ferrer, S.M. Chatman, J.C. Peters, T.F. Jaramillo, Benchmarking hydrogen evolving reaction and oxygen evolving reaction electrocatalysts for solar water splitting devices, J. Am. Chem. Soc. 137 (2015) 4347–4357, https://doi.org/10.1021/ja510442p.

[66] Y. Yu, W. Zhang, F. Sun, Q. Fang, J. Pan, W. Chen, G. Zhuang, High electrocatalytical performance of FeCoNiCuPd high-entropy alloy for nitrogen reduction reaction, Mol. Catal. 519 (2022) 112141, https://doi.org/10.1016/j.mcat.2022.112141.

[67] M.V. Kante, M.L. Weber, S. Ni, I.C.G. van den Bosch, E. van der Minne, L. Heymann, L.J. Falling, N. Gauquelin, M. Tsvetanova, D.M. Cunha, G. Koster, F. Gunkel, S. Nemšák, H. Hahn, L. Velasco Estrada, C. Baeumer, A high-entropy oxide as high-activity electrocatalyst for water oxidation, ACS Nano 17 (2023) 5329–5339, https://doi.org/10.1021/acsnano.2c08096.

[68] T. Zhang, H.-F. Zhao, K.-Y. Wang, Z.-J. Chen, L. Li, J. Peng, X. Peng, Y.-J. Huang, H.-B. Yu, Three factors make bulk high-entropy alloys as effective electrocatalysts for oxygen evolution, Mater. Futures 2 (2023) 045101, https://doi.org/10.1088/2752-5724/aceef3.

[69] H. Li, Y. Han, H. Zhao, W. Qi, D. Zhang, Y. Yu, W. Cai, S. Li, J. Lai, B. Huang, L. Wang, Fast site-to-site electron transfer of high-entropy alloy nanocatalyst driving redox electrocatalysis, Nat Commun 11 (2020) 5437, https://doi.org/10.1038/s41467-020-19277-9.

[70] Y. Yang, H. Yao, Z. Yu, S.M. Islam, H. He, M. Yuan, Y. Yue, K. Xu, W. Hao, G. Sun, H. Li, S. Ma, P. Zapol, M.G. Kanatzidis, Hierarchical nanoassembly of MoS2/Co9S8/Ni3S2/Ni as a highly efficient electrocatalyst for overall water splitting in a wide pH range, J. Am. Chem. Soc. 141 (2019) 10417–10430, https://doi.org/10.1021/jacs.9b04492.

[71] M. Shi, T. Tang, L. Xiao, J. Han, X. Bai, Y. Sun, S. Chen, J. Sun, Y. Ma, J. Guan, Nanoflower-like high-entropy Ni–Fe–Cr–Mn–Co (oxy)hydroxides for oxygen evolution, Chem. Commun. 59 (2023) 11971–11974, https://doi.org/10.1039/D3CC04023B.